Biophysical Journal, Volume *111*

Supplemental Information

A Coiled-Coil Peptide Shaping Lipid Bilayers upon Fusion

Martin Rabe, Christopher Aisenbrey, Kristyna Pluhackova, Vincent de Wert, Aimee L. Boyle, Didjay F. Bruggeman, Sonja A. Kirsch, Rainer A. Böckmann, Alexander Kros, Jan Raap, and Burkhard Bechinger

Supporting Material

A Coiled-Coil Peptide Shaping Lipid Bilayers upon Fusion

Martin Rabe[a,b,*], *Christopher Aisenbrey*[c], *Kristyna Pluhackova*[d], *Vincent de Wert*[a], *Aimee L. Boyle*[a], *Didjay F. Bruggeman*[a], *Sonja A. Kirsch*[d], *Rainer A. Böckmann*[d], *Alexander Kros*[a]; *Jan Raap*[a], and *Burkhard Bechinger*[c,*]

[a] Leiden Institute of Chemistry – Supramolecular and Biomaterial Chemistry, Leiden University, Einsteinweg 55, 2333CC Leiden, The Netherlands.

[b] Present address: Max-Planck-Institute für Eisenforschung GmbH, Department of Interface Chemistry and Surface Engineering, Max-Planck-Str. 1, 40237 Düsseldorf, Germany.

[c] Université de Strasbourg/CNRS UMR7177, Institut de Chimie, 4, rue Blaise Pascal, F-67070 Strasbourg, France.

[d] Computational Biology, Department of Biology, University of Erlangen-Nürnberg, Staudtstr. 5, 91058 Erlangen, Germany

S1: Influence of E and K labeling on coiled-coil formation

To test whether the synthesized peptides readily form hetero coiled-coil complexes with one binding partner being tryptophan labeled, CD spectroscopy was employed. The UV-CD spectrum of E*/K* at 25 °C is typical for peptides with high α-helical content, showing two minima around 208 and 222 nm, while the spectra of the isolated peptides E* and K* are typical for less helical structures (Figure S1).(1-3) The helical content was estimated from the ellipticity at 222 nm ($[\theta]_{222nm}$). (1, 2) The helicity was found to increase from 21% and 33% for E* and K* respectively, to 83% for the E*/K* complex. Also the formation of E*/K and K*/E complexes could be observed based on spectra representing high helical content with 74% and 75%, respectively (Figure 2A). Under the same conditions E, K, and E/K showed helicities of 21%, 23%, and 72% respectively (spectra not shown). The increasing helical contents prove the interactions between the peptide chains that are accompanied by folding into more helical structures, i.e. formation of the coiled-coil complexes.

The increase in the helical content of E*/K* in comparison to E*/K and E/K* can indicate a higher population of the coiled-coils i.e. a higher folding constant or a higher helicity of the individual coiled-coils or both. In an earlier study we found the folding constant K_F(E*/K*) to be ~3.2 10^7 M^{-1}(4). Which is slightly higher then reported by Litowski and Hodges for E/K: ~1.4 10^7 M^{-1} (5). In the heptad repeat, the tryptophan residues of E* and K* are in the a-position, meaning they can contribute to the hydrophobic binding or even π-stack in the coiled-coil. Such effects increase the dimeric binding and thus the folding.

A higher ellipticity of the individual dimers might be caused by the elongated chain of E*/K*. It is known that coiled coil and short helical peptides fray at the chain ends and thus terminal variations can influence the measured helicity.(6, 7) The terminal tryptophans might reduce this fraying because they can contribute to the coiled-coil interactions. This would lead to a higher ratio of helical to random residues. From the data presented here it is not possible to distinguish these two possible reasons and most likely both effects play a role.

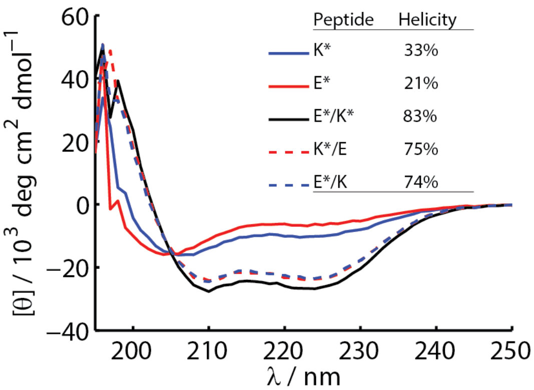

Figure S1. CD spectra of K*, E*, and, the coiled coil complexes E*/K*, K*/E and E*/K at 50 µM total peptide concentrations and 25°C. Values of helicity calculated from $[\theta]_{222nm}$ are shown in the inset table.

In PBS both, K* and E* show similar fluorescence emission spectra with the maxima of their emission (λ_{max}) at 345 nm (Figure S2A). The formation of the complexes E*/K and K*/E by addition of the respective binding partner in equimolar concentrations caused no significant changes in the fluorescence spectra (Figure S2B). Thus, the C-terminus of the peptides is not involved in the hydrophobic binding of the E*/K and K*/E coiled-coil complexes. For comparison Figure S2 displays spectra after addition of vesicles which were altered significantly in case of K* and K*/E. These effects are discussed in detail in the main part of the paper.

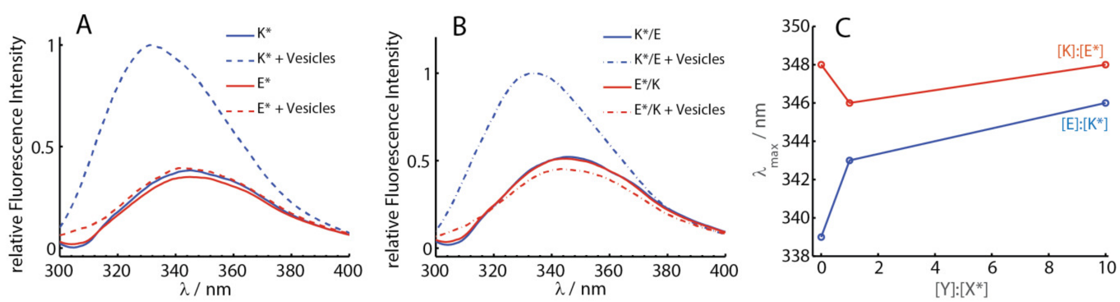

Figure S2. Fluorescence emission spectra of (A) peptides K* and E* in absence and presence of lipid vesicles and of (B) the peptide complexes K*/E and E*/K ([X*]:[Y] = 1:1). Spectra with vesicles at [Lipid]:[X*]=2000:1. (C) Fluorescence emission maxima with increasing amount of coiled coil binding partner in presence of lipid vesicles [Lipid]:[X*]=1000:1.

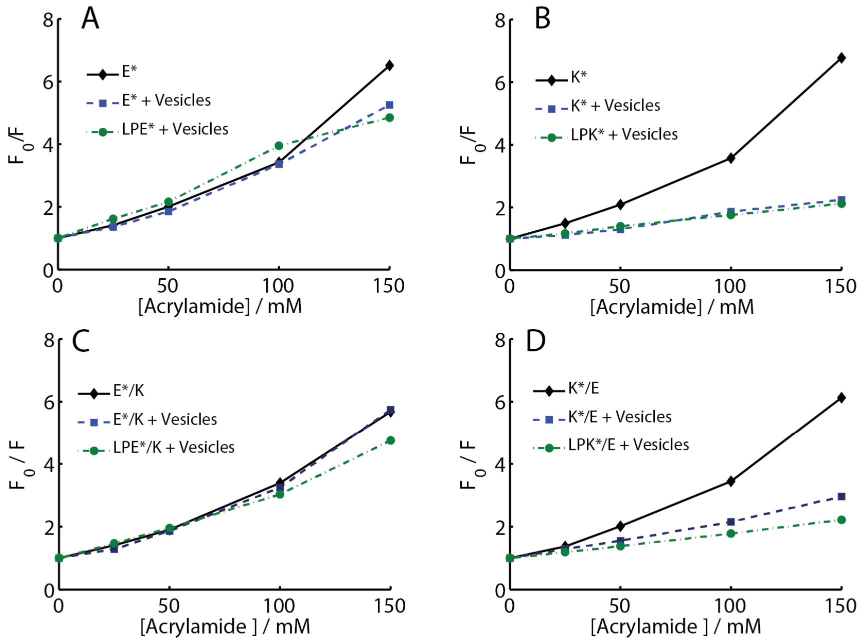

Figure S3. Tryptophan fluorescence quenching by acrylamide. (A & B) Peptides and Lipopeptides with or without vesicles (C & D) Peptide mixtures or lipopeptide-peptide mixtures with or without vesicles. Conditions: [X*] and [LPX*] = 2,5 µM; [Lipid]:[X*] = 1000:1; [Lipid]:[LPX*] = 100:1 (X = E or K respectively), peptide mixtures always 1:1. Vesicles in all experiments are composed of DOPC:DOPE:Cholesterol (2:1:1).

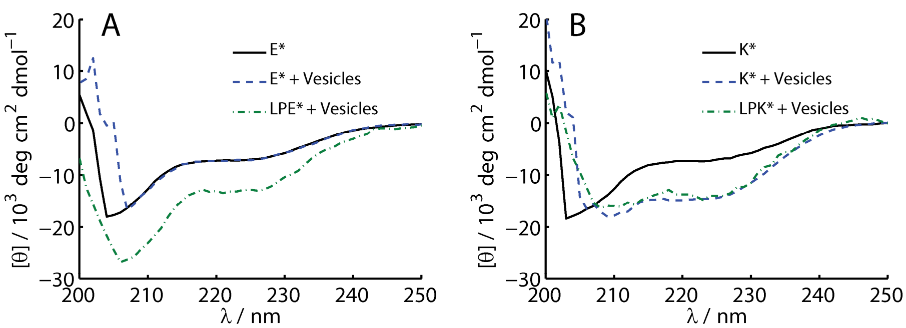

Figure S4. CD spectra of peptides and lipopetides with and without vesicles. (A) E* and LPE*. (B) K* and LPK*. [X*] =5 µM; [Lipid]:[X*]=100:1; [LPX*]=2,5 µM, [Lipid]:[LPX*]= 100:1 (X = E or K respectively).

S2: Analysis of peptide membrane penetration fluorescence data

It has to be assumed that the distance of the bromine moieties from the center of the bilayer is the same in the lipid bilayers used in the present study as in pure di-BrPC bilayers, which were used for determination of the depth of the bromine labels. However precise determination of the bilayer thickness requires diffraction experiments and the available data in the literature is limited. McIntosh and Holloway determined, by x-ray diffraction, the headgroup distance in pure di-BrPC bilayers by x-ray diffraction to be ~40 Å for 6, 7- and 11, 12 – diBrPC.(8, 9) Hung *et. al.* studied bilayers of a DOPC:Cholesterol (3:1) mixture in a fluid state, which is comparable to the mixture used in the present study and determined the distance between the phosphate groups to be ~40 Å as well,(10) showing that the assumption of equal thicknesses is reasonable.

To estimate the distance of the fluorophore from the center of the bilayer Z_{cf} the parallax method(9, 11) was applied using the fluorescence intensities of shallower F_1 and deeper quencher F_2:

$$Z_{cf} = \frac{-\frac{1}{\pi C}\ln\left(\frac{F_1}{F_2}\right) - L_{21}}{2L_{21}} + L_{c1} \tag{S1}$$

where C is the molar fraction per lipid area (~60 Å^2)(10), L_{21} is the distance between deeper and shallower quencher, and L_{c1} is the distance between shallow quencher and bilayer center. For PM the fluorescence intensities of the two closest quenchers were used only. Using the results of 6,7- and 9, 10-diBrPC, PM yields distances of 13.4 Å and 20.2 Å of the indole ring of K* and LPK* from the center of the bilayer.

The distribution analysis method (DA) is generally considered to better reflect the physics of the quenching, due to the disordered nature of the lipid bilayer. Also, it can be applied for quenchers with larger distances to the fluorophore as well as in cases of incomplete binding.(11, 12) For application of the DA, the quenching profile QP as function of the distance to the bilayer center h was fitted by two symmetric Gaussians:

$$QP = \frac{F_0}{F} - 1 = \frac{S}{\sigma\sqrt{2\pi}} e^{-\frac{(h-h_m)^2}{2\sigma^2}} + \frac{S}{\sigma\sqrt{2\pi}} e^{-\frac{(h+h_m)^2}{2\sigma^2}} \tag{S2}$$

the parameter h_m stands for the most probable distance between fluorophore and bilayer center, S is the area and σ the dispersions of the Gaussians.

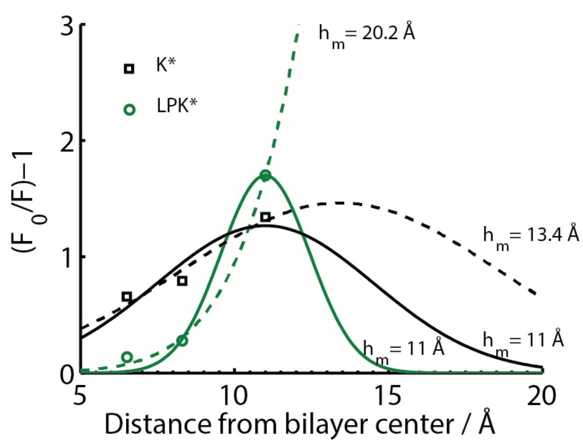

Figure S5. Analysis of depth dependent quenching profiles, using different h_m values. Corresponding values of σ and S are given in Table S1.

The depth dependent quenching profiles of LPK* and K* and the DA are depicted in Figure S5. Due to the little number of data points, which all appear to be on the same flank of one

Table S1. Parameters used for distribution analysis.

	h_m / Å	σ/ Å	S / Å
K*	11,0[a]	3,5	11,2
	13,4[b]	5,1	18,8
LPK*	11,0[a]	1,4	6,1
	20,2[b]	4,1	222,3

[a]distance to the bilayer center of shallowest quencher; [b] Z_{cf} calculated by parallax method with F_1 and F_2 of the quenchers closest to the fluorophore

Gaussian, at least one parameter had to be fixed during regressions. The penetration depths h_m were fixed at different values to assess the influence on the fitted profiles and to evaluate the implications of the resulting models (Table S1). In this way reasonable simulations of the quenching profiles were obtained for $h_m \geq 11$ Å, the position of the most shallow quencher (Figure 4B). Therefore it can be concluded that the most probable depth of the indole side chain of tryptophan in the bilayer is not deeper than 11 Å from the bilayer center.

Fixing the parameter h_m at the values obtained from PM (13.4 Å and 20.2 Å) yielded a reasonable fit of the quenching profile for K* (Figure S5), while for LPK* a very large profile that appears unlikely if compared to profiles found in comparable quenching experiments was obtained. (12) However, if one directly compares the quenching profiles for K* and LPK* and their fits with h_m = 11 Å it becomes clear that the profile for LPK* must be more narrow than for K* i.e. σ must be significantly smaller, which might indicate less conformational freedom of the peptide.(11)

S3: Supporting ^{31}P-NMR data

Figure S6 shows proton-decoupled ^{31}P spectra of unoriented POPC/POPE/cholesterol samples in the presence of the indicated amount of peptide. The sample consists of hydrated lipid films. The addition of peptide results in only small differences in spectral line shapes indicating that the ^{31}P CSA tensors are widely unaffected.

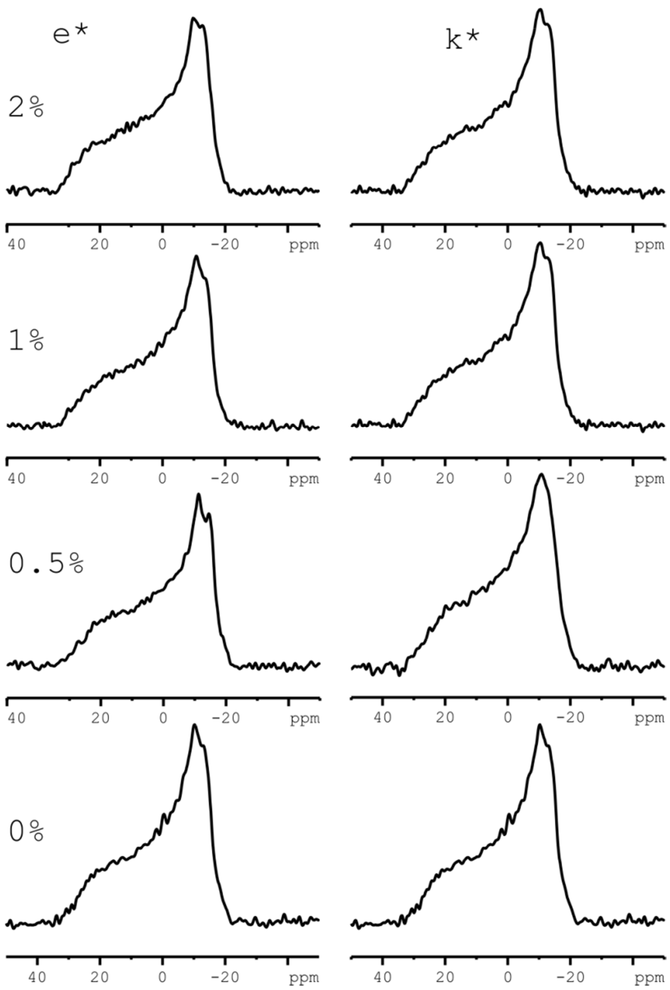

Figure S6: Static solid phase ^{31}P-NMR spectrum of E* and K* peptides in POPC:POPE:Cholesterol (2:1:1) vesicular membranes

In order to verify the assignment of the ^{31}P CSA tensor elements to the individual lipids oriented samples of varying composition were investigated (Figure S7). The spectra allow the assignment of the POPC resonance to 32ppm and 15ppm for $\sigma^{\perp}$ and $\sigma\|$, whereas the POPE resonances were assigned to 25ppm and 10ppm for $\sigma^{\perp}$ and $\sigma\|$.

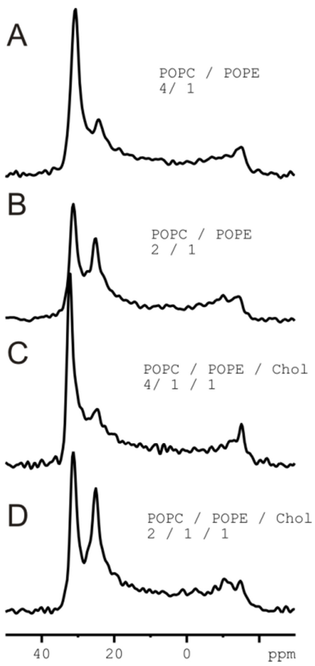

Figure S7: Assignment of the peaks to individual lipids. Proton-decoupled ^{31}P solid-state NMR spectra of supported lipid bilayers prepared from vesicle suspensions made of (A) POPC:POPE 4:1, (B) POPC:POPE 2:1, (C) POPC:POPE:Cholesterol 4:1:1, (D) POPC:POPE:cholesterol 2:1:1.

S4: supporting ^{2}H-NMR data

Deuterium spectra of oriented samples of POPC/POPE/Cholesterol 2/2/1 containing POPC-D_{31} were measured in the presence of increasing amount of peptide (Figure S8). The spectra exhibit a slight increase of the order parameters for low concentration of the peptides (0.5%) before the order parameter return to the original value at higher peptide concentrations.

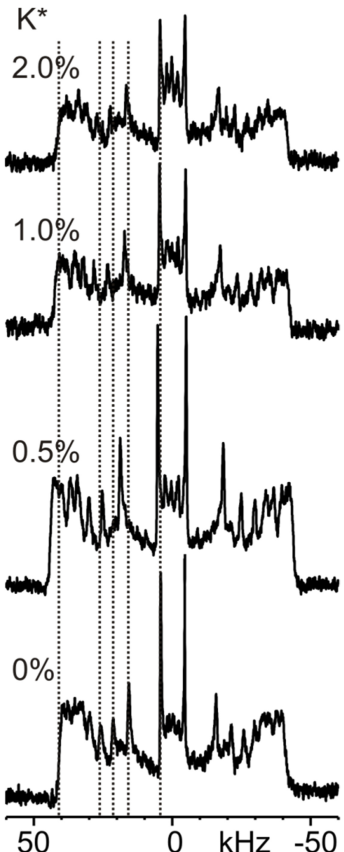

Figure S8. ^{2}H-NMR of an oriented sample of different concentrations of K* in POPC/POPE/Chol 2/2/1 mixed with 10% of palmitoyl perdeuterated POPC.

S5: MD simulations

Curvature effects of peptide K on coarse-grained lipid bilayer

For the study of a curvature-inducing effect of K on a bilayer, systems were prepared including one finite membrane patch and varying amounts of pre-adsorbed peptides to either one or both membrane leaflets. All systems were generated by multiplication of a smaller system in x- and y-direction, thus yielding membrane patches with peptide to lipid ratios ranging from 0:1150 to 1:35 (see Table S2). The basic building block was selected from a previously performed (13) coarse-grained simulation (using the Martini2.2.p force field (14), polarizable water (15), and PME to describe electrostatics) containing one peptide in a fully helical state, which spontaneously adsorbed onto a bilayer that consists of DOPC:DOPE:Cholesterol in a ratio of 2:1:1. The orientation of the peptide on the bilayer agrees well with predictions based on the amphiphatic character of the peptide, I.e. the hydrophobic residues are buried in the membrane, the snorkeling lysines line the peptide on the side and the negatively charged glutamic acids point to the solution. To prevent the influence of periodic boundaries on the bilayer behavior, the simulation box size was adjusted to be larger than the membrane patch, thus resulting in a bilayer patch fully surrounded by water. Furthermore, a salt concentration of 150 mM was set and counter ions were added to neutralize the systems. Simulations were conducted using GROMACS 4.6(16) and the polarizable MARTINI force field.(14, 15) The system was energy minimized using the steepest-descent algorithm and a short 100 ps equilibration simulation was performed. Production simulations were carried out at 1 bar (time constant of 3 ps) with the Berendsen coupling scheme(17) and the temperature was maintained at 310 K by the v-rescale thermostat(18) and a time constant of 1 ps. Long range electrostatic interactions were calculated using the particle-mesh Ewald summation (19) with a real space cutoff of 1.2 nm. The relative dielectric constant was globally set to 2.5. Van der Waals interactions were described by a Lennard Jones 12-6 potential, which was shifted to zero between 0.9 and 1.2 nm. In addition to the aforementioned starting structures 4 simulations (at 310 K and 298 K two each) were performed with only a single peptide adsorbed on the bilayer patch. For this purpose, all membrane-bound peptides except for one were removed from the patch, which was obtained after 200 ns simulation of 8 peptides bound to each monolayer.

The simulation length varied (Table S2) due to different vesiculation speed at different protein:lipid ratios. Each simulation type was conducted twice with different initial starting velocities.

The vesiculation process took place in a similar manner irrespectively of presence or absence of adsorbed peptides K. Generally, a planar patch (side view in Figure S9 A) starts bending already within first nanoseconds of the simulation (Figure S9 B) until the rims approach each other to allow for the formation of a complete vesicle (Figure S9 C).

The duration of this process and the bending direction of the patch varied for different simulated systems. In case of a pure reference bilayer, complete vesicles formed within 140 and 172 ns, respectively (see Table S2), and the bending took place to both sides (to the top and to the bottom, seen from the side). The presence of a high amount of pre-adsorbed peptides K onto the upper monolayer significantly sped up the vesiculation process; here, vesicles formed within less than 65 ns. In all simulations with bound peptides, the rims bend in direction to the peptide-free leaflet, resulting in vesicles with peptides bound to the vesicle's outer monolayer (see Figure S9 C). Similar to observations at high concentration of bound peptides, one single peptide K also accelerates the vesiculation process compared to the peptide-free simulations. Moreover, the vesiculation process is faster at higher temperature.

The attachment of the same amount of K to both monolayers (8 or 16 peptides per monolayer, see Table S2) stabilizes the membrane patch in three out of four simulations for 400 ns. In one simulation vesicle was formed after 205 ns resulting from the travelling of the majority of the peptides from one leaflet over the patch rims to the (future) outer leaflet, and thus significantly increasing the protein:lipid ratio on one bilayer leaflet. It is interesting to note that two peptides remained trapped inside the vesicle.

To summarize, adsorbed peptides K adsorbed on one membrane leaflet induce positive curvature and induce patch vesiculation. The vesiculation time is the shorter the more peptides are adsorbed. These findings suggest a peptide-induced local positive curvature, which facilitates membrane bending and can aid the fusion process.

Table S2: Coarse-grained simulation systems, simulation conditions, and vesiculation times. For each simulation setup two independent simulations were performed.

Peptides number bound to upper/lower monolayer	**Temperature [K]**	**Simulation length [ns]**	**Peptide:lipid ratio**	**Vesiculation time [ns]**
8/0	310	2x100	1:140	65 / 65
16/0	310	2x100	1:70	65 / 62
16/16	310	2x400	1:35	- / -
8/8	310	2x400	1:70	205 / -
0/0	310	2x200	0:1150	172 / 140
1/0	310	2x200	1:1150	85 / 126
1/0	298	2x200	1:1150	125 / 178

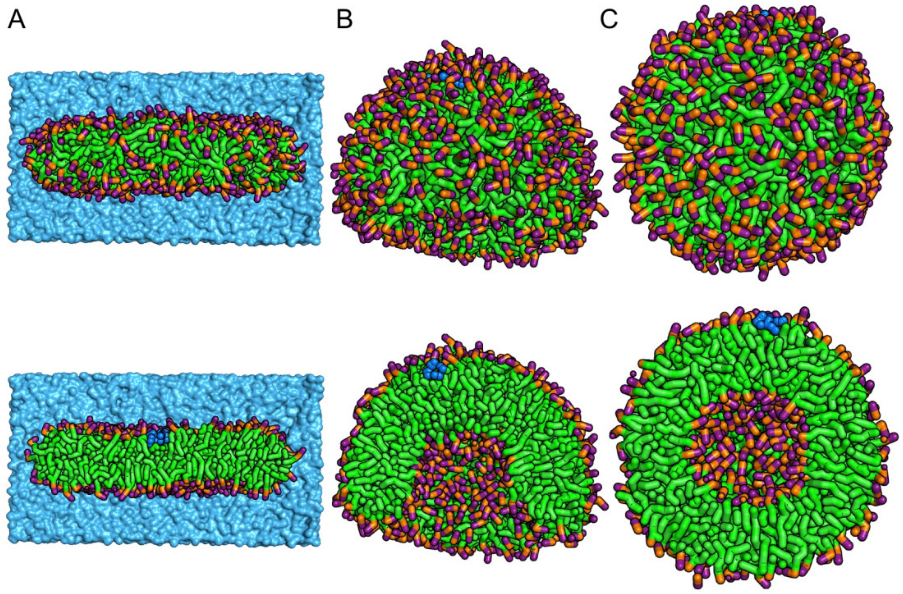

Figure S9. Vesicle formation CG-MD simulations. (A) Membrane patch (B) curved membrane patch (C) Vesicle. Lower row of pictures shows cross sections of the structures in the top. Amino and phosphate headgroup beads are colored in violet and orange, respectively, lipid tails in green. The membrane adsorbed peptide K is shown in blue. Surrounding water is except for subset A omitted for clarity.

Lipid accumulation around peptide K adsorbed on CG vesicles

In presence of multiple copies of peptide K on a vesicle, the average ratio between DOPE and DOPC lipids around peptide K is comparable to their ratio in the whole system (Figure S10). Thus, no preference of one lipid type to accumulate around the peptide was observed in those simulations. Interestingly, in presence of only one peptide K, adsorbed initially on a free patch and later on the developed vesicle, DOPE lipids accumulated in the vicinity of peptide K in 2 out of 4 simulations (see Figure 9c). Similar accumulation was observed in curved atomistic simulations as described in the main text.

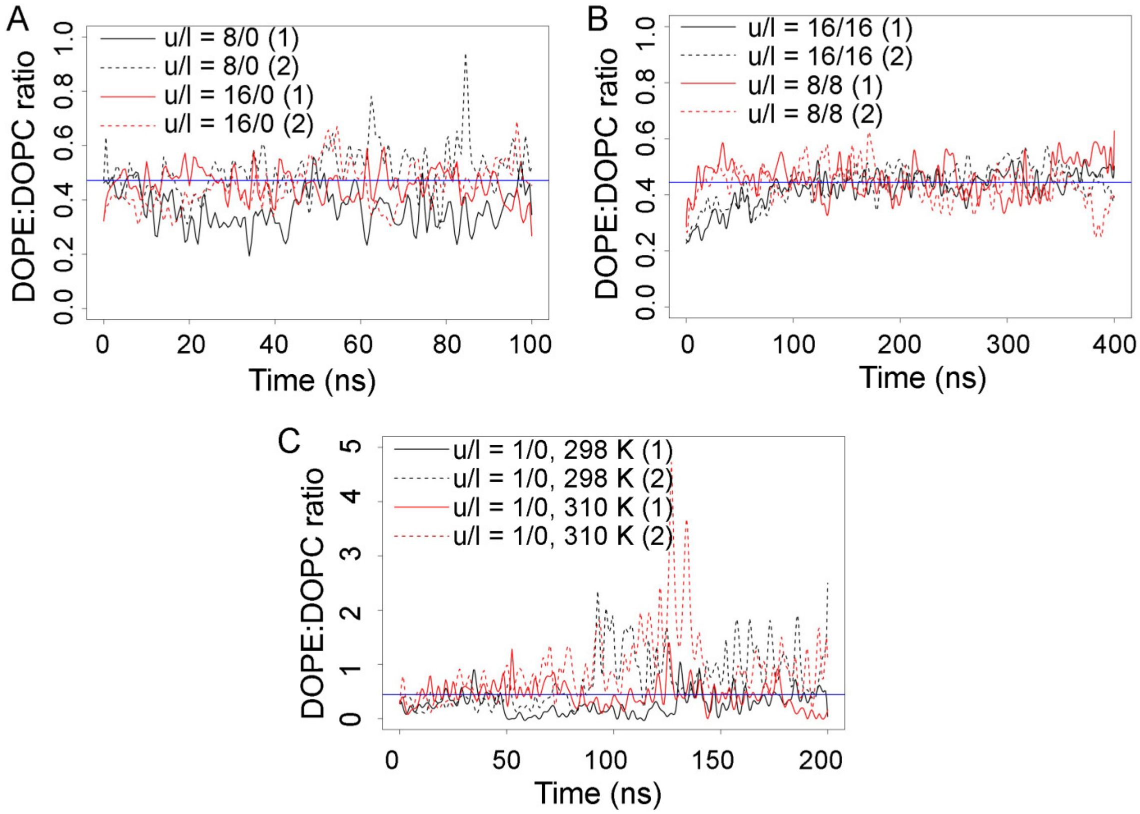

Figure S10. DOPE:DOPC ratio in the vicinity of peptide K. Horizontal blue lines indicate the lipid ratio in the system (DOPE:DOPC ~ 1:2). (A) multiple peptides (8 or 16) adsorbed on one leaflet, (B), multiple peptides (8 or 16) adsorbed on each leaflet (C) one single peptide adsorbed on the outer leaflet. Legend u/l describes how many peptides were adsorbed in the beginning of the simulation on the upper and on the lower layer, respectively. The label (1) and (2) points to two copies of the simulations performed.

Peptides' orientation on the bilayer and secondary structure content in atomistic simulations

As shown in Figure S11 both peptides K are adsorbed on the bilayer in a conformation which is in agreement with the predictions based on the amphiphatic character of the peptide. The hydrophobic residues (leucine and isoleucine) are most deeply inserted, the snorkeling lysines line the peptides on the sides and the negatively charged glutamic acids point to the solution. The peptides exhibit a large amount of helical secondary structure (in average 79% for each peptide). This value is higher than the helicity of membrane bound K* that can be estimated to be ~60%, based on the values given in Table 1 of the main paper, the partitioning coefficient K_P and the folding constant of K* homocoils $K_f = 3420\ M^{-1}$ (4).

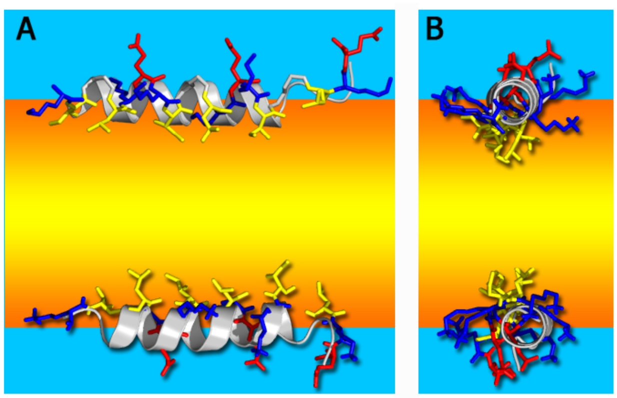

Figure S11. Orientation and secondary structure of peptides K on the bilayer at 300 ns snapshot of the double peptide atomistic simulation. A. view perpendicular to the longest helical axes and B. view along the helix. The membrane is depicted as orange-yellow-orange gradient (with yellow color highlighting the hydrophobic center of the bilayer) and water is shown as cyan background. The peptides secondary structure is shown as grey cartoon and the positioning of the sidechains as color coded sticks. Leucine and isoleucine residues are shown in yellow, lysines in blue, and glutamic acids in red.

Lipid acyl chain protrusion probabilities and membrane dehydration

Table S3. Lipid chain protrusion probabilities in atomistic simulation. *Free* denotes peptide free membrane leaflet and *bound* denotes peptide bound membrane leaflet.

Simulated system	Lipid/leaflet	Average protrusion time [ps]	Number of protrusions [$lipid^{-1}\mu s^{-1}$]	Protrusion efficiency [$\times 10^{-3} lipid^{-1}$]	Coordinated H_2O per P-atom
pure bilayer	DOPC/free	345.0	1.065	0.357	6.636±0.039
	DOPE/free	313.3	1.574	0.493	6.742±0.064
single peptide	DOPC/free	381.8	1.019	0.389	6.640±0.044
	DOPE/free	383.3	1.111	0.426	6.765±0.070
	DOPC/bound	500.0	0.833	0.417	6.406±0.045
	DOPE/bound	787.5	1.296	1.021	6.468±0.097
double peptide	DOPC/bound	529.8	1.529	0.846	6.509±0.029
	DOPE/bound	500.9	1.619	0.811	6.554±0.050

Table S3 shows a summary of lipid protrusion characteristics observed in all-atom simulations. The average protrusion time, the number of protrusion events as well as the protrusion efficiency (resulting from a multiplication of the average protrusion time and the number of protrusion events) are given for each simulated system and in case of the single peptide system for individual peptide bound or peptide free leaflets. Additionally, the lipid headgroup hydration is evaluated as the average number of water molecules coordinated in the first solvation shell around the phosphorous atom of the given lipid type.

S6: Supporting Literature

1. Chen, Y.-H., J. T. Yang, and K. H. Chau. 1974. Determination of the helix and β form of proteins in aqueous solution by circular dichroism. Biochemistry 13:3350-3359.
2. Gans, P. J., P. C. Lyu, M. C. Manning, R. W. Woody, and N. R. Kallenbach. 1991. The helix–coil transition in heterogeneous peptides with specific side-chain interactions: Theory and comparison with CD spectral data. Biopolymers 31:1605-1614.
3. Greenfield, N. J. 2006. Using circular dichroism spectra to estimate protein secondary structure. Nat. Protoc. 1:2876-2890.
4. Rabe, M., A. Boyle, H. R. Zope, F. Versluis, and A. Kros. 2015. Determination of oligomeric states of peptide complexes using thermal unfolding curves. Biopolymers 104:65-72.
5. Litowski, J. R., and R. S. Hodges. 2002. Designing heterodimeric two-stranded alpha-helical coiled-coils. Effects of hydrophobicity and alpha-helical propensity on protein folding, stability, and specificity. J. Biol. Chem. 277:37272-37279.

6. Dragan, A. I., and P. L. Privalov. 2002. Unfolding of a Leucine zipper is not a Simple Two-state Transition. J. Mol. Biol. 321:891-908.
7. Fesinmeyer, R. M., E. S. Peterson, R. B. Dyer, and N. H. Andersen. 2005. Studies of helix fraying and solvation using 13C′ isotopomers. Protein Sci. 14:2324-2332.
8. McIntosh, T. O., and P. W. Holloway. 1987. Determination of the depth of bromine atoms in bilayers formed from bromolipid probes. Biochemistry 26:1783-1788.
9. Chattopadhyay, A., and E. London. 1987. Parallax method for direct measurement of membrane penetration depth utilizing fluorescence quenching by spin-labeled phospholipids. Biochemistry 26:39-45.
10. Hung, W.-C., M.-T. Lee, F.-Y. Chen, and H. W. Huang. 2007. The Condensing Effect of Cholesterol in Lipid Bilayers. Biophys. J. 92:3960-3967.
11. London, E., and A. S. Ladokhin. 2002. Measuring the depth of amino acid residues in membrane-inserted peptides by fluorescence quenching. In Curr. Top. Membr. T. J. M. Sidney A. Simon, editor. Academic Press. 89-115.
12. Ladokhin, A. S. 2014. Measuring membrane penetration with depth-dependent fluorescence quenching: Distribution analysis is coming of age. Biochim. Biophys. Acta 1838:2289-2295.
13. Pluhackova, K., T. A. Wassenaar, S. Kirsch, and R. A. Böckmann. 2015. Spontaneous Adsorption of Coiled-Coil Model Peptides K and E to a Mixed Lipid Bilayer. J. Phys. Chem. B 119:4396-4408.
14. de Jong, D. H., G. Singh, W. F. D. Bennett, C. Arnarez, T. A. Wassenaar, L. V. Schäfer, X. Periole, D. P. Tieleman, and S. J. Marrink. 2013. Improved Parameters for the Martini Coarse-Grained Protein Force Field. J. Chem. Theory Comput. 9:687-697.
15. Yesylevskyy, S. O., L. V. Schäfer, D. Sengupta, and S. J. Marrink. 2010. Polarizable Water Model for the Coarse-Grained MARTINI Force Field. PLoS Comp. Biol. 6:e1000810.
16. Hess, B., C. Kutzner, D. van der Spoel, and E. Lindahl. 2008. GROMACS 4: Algorithms for Highly Efficient, Load-Balanced, and Scalable Molecular Simulation. J. Chem. Theory Comput. 4:435-447.
17. Berendsen, H. J. C., J. P. M. Postma, W. F. van Gunsteren, A. DiNola, and J. R. Haak. 1984. Molecular dynamics with coupling to an external bath. J. Chem. Phys. 81:3684-3690.
18. Bussi, G., D. Donadio, and M. Parrinello. 2007. Canonical sampling through velocity rescaling. Journal of Chemical Physics 126:014101.
19. Darden, T., D. York, and L. Pedersen. 1993. Particle mesh Ewald: An N·log(N) method for Ewald sums in large systems. J. Chem. Phys. 98:10089-10092.